Inhibition of Bacteriophage λ Protein Phosphatase by Organic and Oxoanion Inhibitors†

Nicholas J. Reiter, Daniel J. White, and Frank Rusnak*

Section of Hematology Research and Department of Biochemistry and Molecular Biology, Mayo Clinic and Foundation, Rochester, Minnesota 55905

Received July 30, 2001; Revised Manuscript Received November 16, 2001

ABSTRACT: Bacteriophage λ protein phosphatase (λPP) with Mn^{2+} as the activating metal cofactor was studied using phosphatase inhibition kinetics and electron paramagnetic resonance (EPR) spectroscopy. Orthophosphate and the oxoanion analogues orthovanadate, tungstate, molybdate, arsenate, and sulfate were shown to inhibit the phosphomonoesterase activity of λPP, albeit with inhibition constants (K_i) that range over 5 orders of magnitude. In addition, small organic anions were tested as inhibitors. Phosphonoacetohydroxamic acid (PhAH) was found to be a strong competitive inhibitor ($K_i = 5.1 \pm 1.6$ μM) whereas phosphonoacetic acid ($K_i = 380 \pm 45$ μM) and acetohydroxamic acid ($K_i > 75$ mM) modestly inhibited λPP. Low-temperature EPR spectra of Mn^{2+}-reconstituted λPP in the presence of oxoanions and PhAH demonstrate that inhibitor binding decreases the spin-coupling constant, *J*, compared to the native enzyme. This suggests a change in the bridging interaction between Mn^{2+} ions of the dimer due to protonation or replacement of a bridging ligand. Inhibitor binding also induces several spectral shifts. Hyperfine splitting characteristic of a spin-coupled $(Mn^{2+})_2$ dimer is most prominent upon the addition of orthovanadate ($K_i = 0.70 \pm 0.20$ μM) and PhAH, indicating that these inhibitors tightly interact with the $(Mn^{2+})_2$ form of λPP. These EPR and inhibition kinetic results are discussed in the context of establishing a common mechanism for the hydrolysis of phosphate esters by λPP and other serine/threonine protein phosphatases.

Eukaryotic serine/threonine phosphoprotein phosphatases utilize a dinuclear metal cluster for catalysis and are involved in the dephosphorylation of a variety of phosphoserine/threonine substrates (*3*−*7*). These enzymes function in crucial cellular processes, including gene expression, cell growth, and cell differentiation. Numerous pathophysiological conditions have been attributed to aberrant regulation of these phosphatases including apoptosis, cardiac hypertrophy, immunosupression, memory loss, and cancer (*8*−*11*).

Serine/threonine phosphoprotein phosphatases fall into two structurally distinct gene families (PPP[1] and PPM) according to nomenclature adopted for human genes (*12*). These phosphatases have also been classified on the basis of their substrate specificity, divalent metal ion dependence, and inhibition by different phosphatase inhibitors (*13*−*16*). Of the enzymes in the PPP family, protein phosphatases 1 (PP1), 2A (PP2A), and calcineurin (PP2B) contain the phosphoesterase sequence motif, $DXH(X)_nGDXXDG(X)_mGNHD/E$ (*5*, *17*, *18*). X-ray structures of PP1 (*3*, *4*), calcineurin (*2*, *19*), and, most recently, bacteriophage λ protein phosphatase (λPP) (*1*), a related serine/threonine phosphoprotein phosphatase of the PPP family, reveal that this phosphoesterase motif forms a β−α−β−α−β secondary structure scaffold that provides ligands for the active site dinuclear metal cofactor. An identical constellation of metal ligands and coordination geometries is found in all three enzymes, with the two metal ions linked by a bridging solvent molecule and a μ-1,1 aspartic acid. Additional metal ligands include two solvent molecules, a histidine, and an aspartic acid to the first metal ion (denoted the M1 metal site) and one solvent molecule, two histidines, and an asparagine to the second metal ion (denoted M2). The active sites of these three enzymes are nearly superimposable, with root-mean-square deviation between active site metals and protein ligands <0.5 Å.[2] The conservation in amino acid sequence, protein fold, and active site structure suggests that phos-

† This work was supported by Grant GM46865 from the National Institutes of Health.

* To whom correspondence should be addressed at the Mayo Clinic and Foundation, 200 First St. S.W., Rochester, MN 55905. Telephone: (507) 284-4743. Fax: (507) 266-9302. E-mail:rusnak@mayo.edu.

[1] Abbreviations: BSA, bovine serum albumin; DTT, dithiothreitol; EDTA, ethylenediaminetetraacetic acid; EPR, electron paramagnetic resonance; PhAH, phosphonoacetohydroxamic acid; λPP, bacteriophage λ phosphoprotein phosphatase; PP1, protein phosphatase 1; PP2A, protein phosphatase 2A; PP2B, calcineurin (protein phosphatase 2B); PPM, eukaryotic Ser/Thr phosphatase subfamily including PP2C; PPP, eukaryotic Ser/Thr phosphatase subfamily including PP1, PP2A, and calcineurin; *p*NPP, *p*-nitrophenyl phosphate; PTP, protein tyrosine phosphatase family; WT, wild type.

[2] The root-mean-square deviation calculation was performed using the SwissPdbViewer (version 3.5) software program. The atomic coordinates of λPP, calcineurin, and PP1 were retrieved from the Research Collaboratory for Structural Bioinformatics (RCSB) Protein DataBank (http://www.rcsb.org/pdb/) under filenames 1G5B, 1AUI, and 1FJM, respectively. Active site metal ions and amino acid residues D20, H22, D49, N75, H139, H186, and H76 of the A, B, and C subunits of crystallized λPP (*1*) were superimposed with active site metal ions and amino acid residues D90, H92, D118, N150, H199, H281, and H151 of the calcineurin A subunit (*2*) and the active site metal ions and amino acid residues D64, H66, D92, N124, H173, H248, and H125 of PP1 (*3*).

10.1021/bi011577b CCC: $22.00
Published on Web 12/21/2001

phomonoester hydrolysis proceeds through a common mechanism in these three enzymes.

Purple acid phosphatases can also be considered to be members of the PPP family of metallophosphoesterase. However, the phosphoesterase motif of purple acid phosphatases, $D(X)_nGDXXY(X)_mGNHD/E$, represents a variation of the motif noted above (*16*). These similarities are reflected in a comparable but not identical active site geometry compared to calcineurin and PP1. In PP1/calcineurin, a histidine ligand to the Fe ion is replaced by a tyrosine residue in the purple acid phosphatases. An additional substitution of a solvent molecule with a histidine ligand results in a net water-for-tyrosine substitution in the Fe coordination sphere of calcineurin/PP1 compared to purple acid phosphatase (*10*).

Mn^{2+} is proposed to be the physiological metal ion cofactor for λPP[3] and is an excellent metal coactivator (*20*). In addition, it has been proven to be a useful active site probe because of its paramagnetic properties. Characterization of the spin-coupled $(Mn^{2+})_2$ center of λPP by electron paramagnetic resonance (EPR) spectrometry has demonstrated that the M1 and M2 metal binding sites exhibit different binding affinities, with the M2 site as the high-affinity site (*21, 22*). These results, along with the recently solved X-ray crystal structure and the biochemical and spectroscopic analysis of proteins in which active site residues were mutated (*1, 22, 23*), have provided considerable mechanistic and structural information. Taken together, these studies confirm λPP as an excellent model of the more complex, eukaryotic Ser/Thr PPases. A study of the interaction of serine/threonine phosphoprotein phosphatases with various inhibitors is important as it may provide clues to the mechanism of phosphate ester hydrolysis (*24, 25*). It is long established that one of the products of the phosphatase reaction, orthophosphate, is a modest inhibitor of PPPs ($K_i \sim 1$ mM) at physiological pH (*20, 26, 27*). Other structural and electronic oxoanion analogues of orthophosphate, such as orthovanadate, molybdate, sulfate, tungstate, and arsenate, also inhibit PPPs and purple acid phosphatases (*20, 26, 28*−*30*).

Crystal structures of oxoanion inhibitors bound to PP1, calcineurin, purple acid phosphatase, alkaline phosphatase, and λPP reveal structures that are likely to mimic reaction intermediates (*1*−*4, 19, 31*−*35*). For example, the structure of λPP with sulfate bound in two different coordination modes gave significant insight into how a phosphoserine or phosphothreonine substrate might be hydrolyzed at the active site of λPP. In one orientation, sulfate was bound terminally to the M2 site, whereas in the other configuration, sulfate is coordinated to both metals in a novel, triply bridged mode. It was hypothesized that these mimicked intermediates along the reaction pathway.In this study, the kinetic and spectroscopic properties of Mn^{2+}-reconstituted forms of λPP in the presence of various inhibitors were studied using phosphatase inhibition kinetics and electron paramagnetic resonance (EPR). A series of organic and oxoanion inhibitors were utilized with the aim of understanding and establishing a mechanism for the hydrolysis of phosphate esters in λPP and other Ser/Thr PPases.

[3] Reiter, T. A., Reiter, N. J., and Rusnak, F., personal communication.

EXPERIMENTAL PROCEDURES

Materials

Ampicillin, Coomassie Brilliant Blue-G250, bovine serum albumin (BSA), dithiothreitol (DTT), $MnCl_2$, *p*-nitrophenyl phosphate, disodium salt (*p*NPP), DEAE-Sephadex CL-6B, phenyl-Sepharose, Dowex 1-Cl (200−400 mesh), Tris, glycerol, phosphonoacetic acid, LiCl, LiOH, acetohydroxamic acid, succinic acid, malonic acid, sodium phosphate (monobasic), sodium molybdate (dihydrate), sodium orthovanadate, sodium sulfate (anhydrous), and sodium tungstate were obtained from Sigma−Aldrich (St. Louis, MO). Hydroxylamine hydrochloride was purchased from EM Science (Cherry Hill, NJ). Ultrafree (5 kDa cutoff) microconcentrators were purchased from Millipore (Bedford, MA). YM10 Diaflo ultrafiltration membranes were purchased from Amicon, Inc. (Beverly, MA). NAP-25 gel filtration columns containing Sephadex G25 resin were purchased from Pharmacia Biotech (Piscataway, NJ). The plasmid pT7-7 was obtained from Stanley Tabor (*36*). Bacterial growth media were purchased from Fisher Scientific Co. (Hanover Park, IL). All chemicals were ACS grade or better, and glass-still-distilled water was used throughout.

Synthesis of Phosphonoacetohydroxamic Acid (PhAH). PhAH was synthesized as previously described (*37*) with the following modifications. Phosphonoacetic acid was converted to the monoethyl ester by refluxing 1.0 g (7.1 mmol) in 50 mL of absolute ethanol with 0.125 mL of H_2SO_4 for 4 h. The solution was cooled, and the monoethyl ester was converted to the hydroxamate by adding 25 mL of a freshly prepared solution of 2.0 M NH_2OH−HCl in 3.0 M NaOH dropwise. After 30 min, the reaction mixture was diluted to 0.85 L, adjusted to pH 8.0 with concentrated HCl, and applied to a 2.5 × 30 cm column of Dowex 1-Cl. The column was washed with 500 mL of water, and PhAH was eluted with a 1.2 L LiCl gradient from 0 to 0.1 M in 20 mM HCl. Fractions (12 mL) were collected and analyzed for PhAH by adding 0.5 mL of each fraction to 0.2 mL of 1% $FeCl_3$ and measuring the absorbance due to the PhAH−Fe complex at $\lambda = 505$ nm. PhAH eluted around 50 mM LiCl. Pooled fractions were adjusted to pH 8.0 using 3 M LiOH, frozen in liquid N_2, and lyophilized. LiCl was removed from the lyophilized powder by washing with dry methanol−acetone (1:4). Filtration using Whatman filter paper and a Buchner funnel recovered the Li^+-hydroxamate salt. Further column purification of the pooled fractions over a second Dowex 1-Cl column allowed for further resolution of PhAH from phosphonoacetic acid. The Li^+ salt was stored desiccated at room temperature with an overall yield of 780 mg (52%). ^1H 300 MHz NMR (in D_2O) showed δ 2.4 (d, $J_{PCH} = 18.6$ Hz) and 92% purity, with phosphonoacetic acid being the major impurity.

Expression and Purification of WT λPP. Expression and purification of bacteriophage λ protein phosphatase were performed as previously described using the plasmid pT7-7 containing the WT λPP DNA sequence transformed into *E. coli* BL21(DE3) cells (*1, 20, 22*). Following growth in 2×TY media containing 400 μg/mL ampicillin in 6 L Erlenmeyer flasks, the cells were lysed and centrifuged and the supernatant was purified using a combination of anion exchange (DEAE Sephadex CL-6B) and hydrophobic interaction

(phenyl-Sepharose) chromatographies. The purified apoenzyme was dialyzed twice against 4 L of 100 mM Tris-HCl, pH 7.8, 100 mM NaCl, 10% glycerol; further concentrated to 19−35 mg/mL using YM-10 Diaflo ultrafiltration membranes (Amicon, Beverly, MA) or Millipore ultrafree concentrators (Bedford, MA); and frozen at −70 °C. Concentrations of protein mixtures and cell extracts were determined using the Coomassie Plus Protein Assay Reagent (Pierce, Rockford, IL), using a BSA as a standard. The concentration of purified protein was also measured in triplicate using $\epsilon_{280} = 41\,700\ M^{-1}\ cm^{-1}$.

Methods

EPR and NMR Spectroscopy. EPR spectra were obtained using a Bruker ESP 300E spectrometer operating at X-band microwave frequency (9.46 GHz) with samples maintained at low temperature (3.3−100 K) using an Oxford Instruments ESR 900 continuous helium flow cryostat. ^{1}H NMR spectra of PhAH were acquired using a Bruker AMX-300 widebore multinuclear spectrometer.

Inhibition Studies of λ Protein Phosphatase. Inhibition of λPP by small organic molecules and oxoanions was performed in 0.1 M Tris-HCl, pH 7.8, 0.1 M NaCl, and 10% glycerol with 1 mM $MnCl_2$, 2.0−90 mM *p*NPP, and approximately 4 nM λPP. Inhibitors were added to the solution with the following concentration ranges: PhAH (0.0−60 μM), phosphonoacetic acid (0.0−2 mM), acetohydroxamate (0.0−500 mM), succinic acid (0.0−25 mM), malonic acid (0.0−20 mM), orthovanadate (0.0−10 μM), tungstate (0.0−200 μM), phosphate (0.0−10 mM), molybdate (0.0−10 mM), sulfate (0.0−60 mM), and arsenate (0.0−20 mM). Vanadate, tungstate, and molybdate in aqueous solution undergo formation of polyoxoanions (*38*). Stock solutions of tungstate, molybdate, orthovanadate, and arsenate were prepared at pH 8.0 to minimize the formation of polyoxoanions. At the concentrations used in this study, the monomer is the predominant species (*39, 40*). Reactions were started upon the addition of λPP, and the reaction was monitored by the increase in absorbance at 410 nm versus time using a Varian Cary 1 double-beam spectrophotometer, with $\epsilon_{410} = 14\,400\ M^{-1}\ cm^{-1}$ for the *p*-nitrophenolate anion at pH 7.8 and 25 °C. The initial velocities at different substrate and inhibitor concentrations were fit to three different kinetic models including competitive, uncompetitive, and mixed (noncompetitive) inhibition using DYNAFIT software on an IBM-compatible personal computer (*41*). The model discrimination analysis method of DYNAFIT was used to distinguish the mode of inhibition.

Time-Dependent Inhibition Study Using PhAH, Orthovanadate, and Tungstate. Progress curves for the reaction of λPP with 20 mM *p*NPP in 0.1 M Tris-HCl, pH 7.8, 0.1 M NaCl, 10% glycerol, and 1 mM $MnCl_2$ were followed spectrophotometrically at 410 nm using concentrations of PhAH, orthovanadate, and tungstate at 0.0, 75, 100, and 200 μM. After an initial assessment of the reaction velocity, the inhibitor was added, and monitoring of *p*-nitrophenolate production was continued.

EPR Analysis of λ Protein Phosphatase Reconstituted with Mn^{2+} (*21, 22*). Recombinant λPP at a final concentration of 120−300 μM (3−7.5 mg/mL) in 0.1 M Tris-HCl, pH 7.8, 0.1 M NaCl, 10% glycerol, and 1 mM $MnCl_2$ was incubated 10−15 h at 4 °C. Following incubation, the protein was concentrated to 0.5 mL using an ultrafiltration cell equipped with a YM-10 membrane. The sample was then exchanged into the same buffer without $MnCl_2$ by passage over a NAP-25 column. The sample was concentrated, measured in triplicate for protein concentration, transferred to a quartz EPR tube, and frozen by immersion in liquid nitrogen. EPR spectra of Mn^{2+}-reconstituted λPP were obtained at 3.5 and 30 K. EPR samples were then thawed, and the following inhibitors were added: arsenic acid (disodium salt) (50 mM), sodium orthophosphate (10 mM), tungstic acid (sodium salt) (2.0 mM), sodium orthovanadate (1.1 mM), and PhAH (840 μM). EPR samples with inhibitors were mixed and incubated at room temperature for 5 min prior to freezing. All EPR samples were prepared from the same batch of purified protein which had a specific activity of $(5.0 \pm 0.5) \times 10^2$ μmol min^{-1} mg^{-1}.

EPR Spectroscopic Analysis of Various Inhibitor Complexes. The magnetic spin levels of high-spin Mn^{2+} ($S = 5/2$) can be described by the spin Hamiltonian, **H** (eq 1) (*42*):

$$\mathbf{H} = D(S_z^2 - S^2) + E(S_x^2 - S_y^2) + g_0\beta\vec{\mathbf{H}}\cdot\vec{\mathbf{S}} + A\vec{\mathbf{S}}\cdot\vec{\mathbf{I}} \quad (1)$$

where D and E represent zero-field splitting terms, g_0 is the intrinsic g value for Mn^{2+}, β is the Bohr magneton, and A is the hyperfine constant describing the strength of the interaction between the electronic spin and the nuclear spin of ^{55}Mn ($I = 5/2$). The zero-field splitting terms D and E split the six m_s levels of the ground-state $S = 5/2$ spin system into three sets of degenerate doublets with $m_s = \pm 1/2$, $\pm 3/2$, and $\pm 5/2$. Application of an external magnetic field completely removes all degeneracies according to the Zeeman interaction. Magnetic coupling between nuclear and electronic spins split each of the electronic levels into 6 additional levels, leading to 36 states, each characterized by electronic (M, m_s) and nuclear (m, m_I) quantum numbers. EPR selection rules ($\Delta m_s = \pm 1$, $\Delta m_I = 0$) result in 30 allowed transitions whose resonance frequency is a function of the orientation of the molecule relative to the external magnetic field. In most cases for Mn^{2+} ions in an all-oxygen/nitrogen coordination environment, the zero-field splitting and Zeeman interactions are of comparable magnitude.

When two paramagnetic Mn^{2+} ions ($S = 5/2$) are bound in close proximity to each other, they can interact via an exchange coupling mechanism. When this occurs, an additional term is added to the spinHamiltonian, given by eq 2.

$$\mathbf{H}' = J\vec{\mathbf{S}}_1\cdot\vec{\mathbf{S}}_2 \quad (2)$$

In eq 2, $\vec{\mathbf{S}}_1$ and $\vec{\mathbf{S}}_2$ represent the spin operators for each high-spin Mn^{2+} ion ($S_1 = S_2 = 5/2$) and the coupling constant J represents the strength of the exchange interaction. When J is the dominant term in the Hamiltonian, a set of spin states with total spin S result, where $S = S_1 + S_2$. S can take on integral values from $|S_1 - S_2|$ to $(S_1 + S_2)$, i.e., $S = 0, 1, 2, \ldots, 5$ for high-spin Mn^{2+}, separating in energy according to eq 3.

$$E = J/2[S(S+1) - (S_1(S_1+1) - S_2(S+1))] \quad (3)$$

For an antiferromagnetically coupled system, the ground state is diamagnetic ($S = 0$) and is EPR-silent while each excited

Table 1: Inhibition of Mn^{2+}-Stimulated λPP *p*NPP Phosphatase Activity by Oxoanions

oxoanions	K_i[a] (μM)	IC_{50}[b] (μM)	X−O bond length (Å)[c]	pK_1[d]	pK_2	pK_3	principal ionized species at pH 7.8
H_3VO_4	0.70 ± 0.20	0.72	1.655 ± 0.095	3.78	7.85	13.0	$(H_2VO_4)^-$ + $(HVO_4)^{2-}$
H_2WO_4	42 ± 13	58	1.757 ± 0.020	4.6	3.5		$(WO_4)^{2-}$
H_3PO_4	710 ± 130	710	1.520 ± 0.047	2.16	7.21	12.32	$(HPO_4)^{2-}$
H_2MoO_4	1300 ± 260	2000	1.762 ± 0.033	3.55	4.2		$(MoO_4)^{2-}$
H_3AsO_4	6000 ± 1400	>1900	1.686 ± 0.027	2.26	6.76	11.29	$(HAsO_4)^{2-}$
H_2SO_4	~20000	18000	1.449 ± 0.030	−3	1.99		$(SO_4)^{2-}$

[a] The value reported for sulfate represents the concentration of inhibitor that leads to 50% inhibition (IC_{50}) and was not evaluated utilizing the DYNAFIT software program. [b] IC_{50} values reported by (*20*). [c] X−O bond lengths ± standard deviation, where X = V, W, P, Mo, As, and S, were obtained by averaging bond lengths from a number of three-dimensional X-ray structures from the Protein DataBank. The following PDB files were used: VO_4, 1RPT, 1IDQ, 1QI9, 3RNT; WO_4, 1ATG, 1WOD, 1FR3; PO_4, 1UTE, 1A2Y, 1A40, 1A54, 1AJK, 1AOP, 1BI2, 1B7D; MoO_4, 1EO1, 1AMF, 1H9J, 1H9M; SO_4, 1QHW, 1G5B, 1FIT, 104M, 1AOJ, 102M, 109M, 1A2Z, 1A3C. Arsenic−oxygen bond lengths for AsO_4 were determined from X-ray structures of arsenate model compounds (*68*−*71*). [d] pK_a values for phosphoric, arsenic, and sulfuric acid were from standard tables of dissociation constants for inorganic acids and bases. pK_a values for vanadic, molybdic, and tungstic acid were from (*40*, *72*).

Table 2: Inhibition of Mn^{2+}-Stimulated λPP *p*NPP Phosphatase Activity by Organic Anions

organic anions	K_i[a] (μM)
phosphonoacetohydroxamate (PhAH)	5.1 ± 1.6
phosphonoacetate	380 ± 45
acetohydroxamate	~75000
succinate	~12000
malonate	~9000

[a] Values reported for acetohydroxamate, malonate, and succinate represent the concentration of inhibitor that leads to 50% inhbition (IC_{50}) and were not evaluated utilizing the DYNAFIT software program.

state ($S = 1, 2, ..., 5$) can give rise to a unique EPR spectrum. Thus, when J is the dominant term in eq 3, the observed EPR spectra are temperature-dependent and will represent a sum of spectra contributed from each spin level weighted according to a Boltzmann population distribution governed by eq 3 and the temperature of the system (eq 4).

$$n_s(T) = \frac{(2S+1)\exp[-S(S+1)J/kT]}{\sum_i (2S_i+1)\exp[-S(S_i+1)J/kT]} \quad (4)$$

RESULTS

Inhibition of λPP by Organic Anions and Oxoanions. A variety of anions were tested as potential inhibitors of λPP. These can be grouped into two categories: oxoanions, as orthophosphate product analogues, and organic anions, which mimic the substrate phosphomonoester or possibly a transition state. Using *p*NPP as substrate, all compounds were shown to inhibit the phosphomonoesterase activity of λPP using Mn^{2+} as the activating metal ion cofactor, albeit with inhibition constants (K_i) that range over 5 orders of magnitude (Tables 1 and 2). Initial reciprocal plots indicated competitive inhibition for all inhibitors. Nevertheless, the entire data set for each was fit to competitive, noncompetitive, and mixed inhibition models using the program DYNAFIT (*41*). This nonlinear, least-squares analysis approach confirmed competitive inhibition for all compounds as the best of these models to describe the data based on the magnitude of the errors. It should be noted that preparations of *p*NPP contain a small amount of contaminating orthophosphate (≈1%), thus complicating the interpretation of data obtained at the highest concentrations of *p*NPP. Despite this, the assumption of competitive inhibition and the use of uniform assay conditions allow a reasonable comparison of the inhibition constants across this series of compounds. Tables 1 and 2 list K_i values for these various inhibitors. DYNAFIT nonlinear plots of initial velocity versus substrate concentration are available in Supporting Information.

Of the oxoanions, orthovanadate ($K_i = 0.70 \pm 0.20$ μM) and tungstate ($K_i = 42 \pm 13$ μM) are both potent inhibitors of λPP (Table 1). These oxoanions do not display time-dependent inhibition upon examining their product progress curves following addition of inhibitor; i.e., the rate of product formation remains constant for up to 18 min, indicating that both of these oxoanions establish a rapid equilibrium with λPP (data not shown). Phosphate ($K_i = 0.71 \pm 0.39$ mM) and molybdate ($K_i = 1.30 \pm 0.26$ mM) behave similarly as competitive inhibitors of λPP but are ~10^3 less effective than orthovanadate. Arsenate ($K_i = 6.0 \pm 1.4$ mM) and sulfate ($K_i \sim 20$ mM) are both poor inhibitors of λPP.

PhAH ($K_i = 5.1 \pm 1.6$ μM) is a strong competitive inhibitor of λPP (Table 2). Removal of the hydroxamate group in PhAH yields phosphonoacetate ($K_i = 380 \pm 45$ μM), which decreases the effectiveness of the inhibitor ~75-fold. Acetohydroxamate ($K_i \sim 75$ mM), which has the phosphonate group missing compared to PhAH, does not readily inhibit phosphate ester hydrolysis of λPP. Therefore, both the hydroxamate and $-PO_3^{2-}$ functional groups are necessary. Additional compounds with bifunctional metal-coordinating moieties, malonic acid and succinic acid, were used to investigate whether small dicarboxylic acids are inhibitors of λPP. They were found to be only weak inhibitors of λPP ($K_i \approx 9$ and 12 mM, respectively).

Progress curves for the reaction of λPP with *p*NPP in the presence of PhAH indicate that PhAH is not a slow, tight binding inhibitor of λPP as previously observed for enolase (*37*). Like orthovanadate and tungstate, the rate of product formation is constant at all times monitored for PhAH concentrations from 0.0 to 200 μM, indicating that PhAH establishes a rapid equilibrium with λPP (data in Supporting Information).

EPR Spectra of Mn^{2+}-Reconstituted λ Protein Phosphatase in the Presence of Inhibitors. It has previously been shown that reconstitution of λPP with Mn^{2+} produces a mixture of two Mn−protein complexes: a mononuclear Mn^{2+} species representing partially occupied enzyme with the Mn^{2+} ion residing in the M2 site, and a fully reconstituted, spin-coupled $(Mn^{2+})_2$ dimer. Each of these species gives rise to unique EPR spectra that can be differentiated based on their

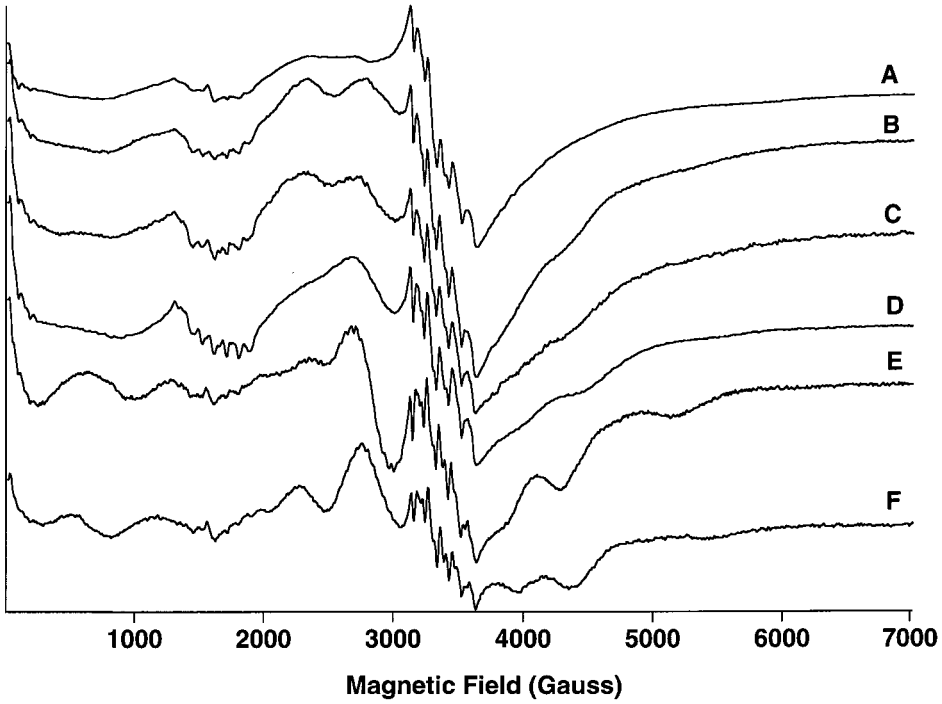

FIGURE 1: Low-temperature EPR spectra of Mn^{2+}-reconstituted λPP in the absence and presence of various inhibitors. (A) WT λPP (1.15 mM) in the absence of inhibitor at 3.3 K. (B) WT λPP (1.08 mM) in the presence of 50 mM arsenate at 3.2 K. (C) WT λPP (1.1 mM) in the presence of 10 mM inorganic phosphate at 3.5 K. (D) WT λPP (2.0 mM) in the presence of 2.0 mM tungstate at 3.2 K. (E) WT λPP (1.01 mM) in the presence of 1.1 mM orthovanadate at 3.2 K. (F) WT λPP (0.85 mM) in the presence of 0.84 mM phosphonoacetohydroxamic acid at 3.5 K. Spectrometer conditions: microwave power, 0.5 mW; microwave frequency, 9.46 GHz; modulation amplitude, 2 G at 100 kHz.

temperature dependence and electron−nuclear hyperfine patterns (*21*, *22*).[4] The intensity of the EPR spectrum of the mononuclear Mn^{2+} species follows a $1/T$ Curie-law dependence and is therefore most intense at the lowest temperature attainable on our spectrometer, ca. 3.2 K. The EPR spectrum of the spin-coupled $(Mn^{2+})_2$ species, on the other hand, results from an excited-state feature, is not observable for temperatures < 7 K, and exhibits maximum intensity at 20−30 K. The spectral features unique to each species have been described previously (*21*). EPR spectra of Mn^{2+}-reconstituted λPP at 4 and 30 K provide representative spectra of the mononuclear Mn^{2+} and dinuclear $(Mn^{2+})_2$ species of the native enzyme, respectively (Figures 1A and 2A). Features representative of the mononuclear Mn^{2+} species include an intense, and nearly isotropic resonance at 3.3 kG with a six-line ^{55}Mn-hyperfine pattern ($g \approx 2$, $A \approx 90$ G), a broad feature extending from 2 to 3 kG, a $\Delta m_s = \pm 2$ transition exhibiting ^{55}Mn-hyperfine-splitting at 1.3−2.1 kG ($g = 4.05$, $A = 88$ G), and a weak, near-zero-field transition also exhibiting ^{55}Mn hyperfine interactions ($g \geq 17$) (*21*, *22*). The same or similar features can also be observed in EPR spectra of Mn^{2+}-reconstituted λPP in the presence of the inhibitors arsenate, phosphate, tungstate, orthovanadate, and PhAH, although the intensities vary from sample to sample (Figure 1, B−F).

Interestingly, several features from a dinuclear $(Mn^{2+})_2$ species are also present in 4 K spectra of the inhibitor complexes of λPP (Figure 1). These include a pair of resonances from 0.3 to 1.4 kG in samples containing vanadate and PhAH (Figure 1, E and F); features at 2.3 and 2.7 kG in samples containing arsenate, phosphate, tungstate, vanadate, and PhAH (Figure 1, B through F); and a series of broad shoulders distinct for each spectrum ranging from 3.8 to >6 kG. Although these new features are better resolved in the 30 K EPR spectra (Figure 2), they are clearly visible in the 4 K EPR spectra of samples containing inhibitors, a distinguishing feature compared to the native Mn^{2+}-reconstituted enzyme (Figure 1A). Many of these features also exhibit ^{55}Mn-hyperfine interactions that are typical of spin-coupled $(Mn^{2+})_2$ dimers, i.e., a splitting approximately half (ca. 40 G) that expected for a monomer.

It is evident that the spectral features noted above, in Figure 1, B through F, are indicative of a spin-coupled $(Mn^{2+})_2$ center of λPP. These resonances arise from excited states, most likely the $S = 2$ manifold of a coupled system (*43*). The fact that they are apparent at 3−4 K indicates that inhibitor binding decreases the spin-coupling constant, J, compared to the native enzyme. In exchange-coupled metal dimers, the coupling constant is dependent upon the nature of the ligand that bridges the two paramagnetic metal ions. In wild-type λPP, a μ-solvent (aquo, hydroxo) ligand is shared between the metal ions (*1*). From EPR studies, the coupling interaction is thought to be antiferromagnetic, with a coupling constant of only a few cm^{-1} (*21*). The change in the coupling constant suggests a change in the bridging interaction between the two paramagnetic metal ions, due either to protonation or to replacement of the bridging ligand.

In the 30 K EPR spectra of Figure 2, many notable differences occur in both the intensities and the resonance positions of the dinuclear $(Mn^{2+})_2$ cluster of native λPP

[4] In addition to these two Mn−protein complexes, a variable amount of free $Mn(H_2O)_6^{2+}$ is also present. EPR spectra of $Mn(H_2O)_6^{2+}$ consist of a 6-line hyperfine pattern centered at $g = 2$ (3450 G) with ca. 90 G spacing between hyperfine lines.

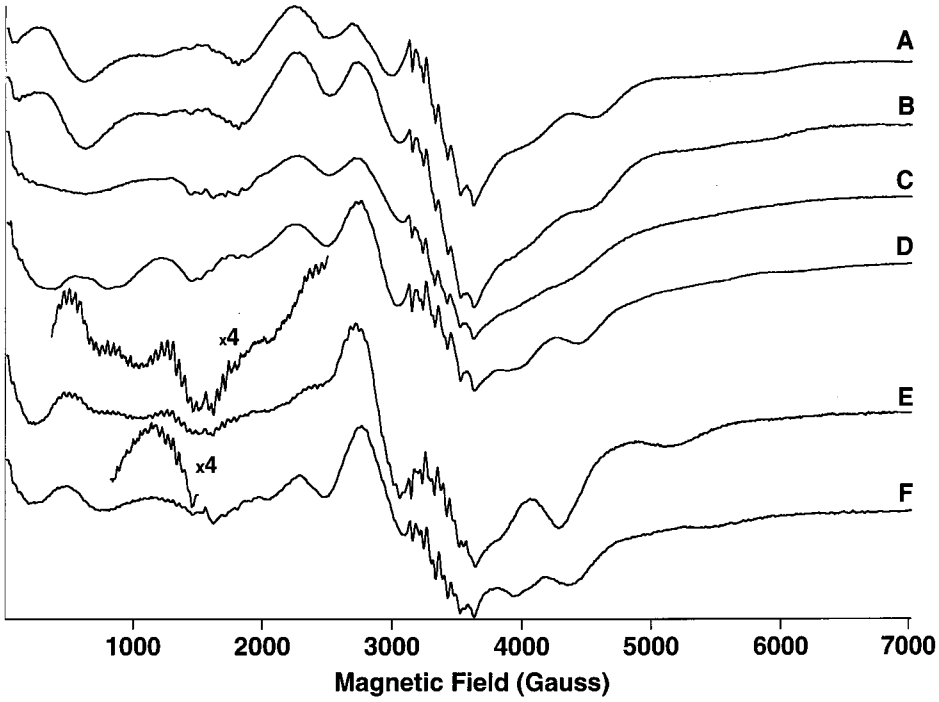

FIGURE 2: 30 K EPR spectra of Mn^{2+}-reconstituted λPP in the absence and presence of various inhibitors. (A) WT λPP (1.15 mM) in the absence of inhibitor. (B) WT λPP (1.08 mM) in the presence of 50 mM arsenate. (C) WT λPP (1.1 mM) in the presence of 10 mM inorganic phosphate. (D) WT λPP (2.0 mM) in the presence of 2.0 mM tungstate. (E) WT λPP (1.01 mM) in the presence of 1.1 mM orthovanadate. (F) WT λPP (0.85 mM) in the presence of 0.84 mM phosphonoacetohydroxamic acid. Spectrometer conditions: microwave power, 20.0 mW; microwave frequency, 9.46 GHz; modulation amplitude, 2 G at 100 kHz.

compared to inhibitor complexes (Figure 2). The addition of 50 mM arsenate (Figure 2B) caused only minor changes in the 30 K EPR spectrum, indicating little alteration of zero-field splitting parameters of either Mn^{2+} ion. Spectral changes which distinguish the phosphate complex (Figure 2C) from the native enzyme (Figure 2A) can be seen by comparing Figure 2, C and A. The most notable difference is the absence of the derivative-shaped feature from 0.1 to 1.0 kG in the phosphate complex. In addition, the three broad high-field resonances in the 4−6 kG region of the native enzyme are shifted to lower field and significantly less resolved in the phosphate complex. Tungstate (2.0 mM, Figure 2D) also results in numerous spectral shifts in both low- and high-field features relative to the native enzyme. The tungstate complex also exhibits an intense near-zero-field transition.

The 30 K EPR spectra of λPP in the presence of orthovanadate (Figure 2E) and PhAH (Figure 2F) are quite distinct from the EPR spectrum of the native enzyme yet remarkably similar to each other. The derivative feature from 0.1 to 1.0 kG of the native enzyme is shifted to 0.35−0.65 kG in these inhibitor complexes. The high-field resonances (4−6 kG) are sharper and more resolved in both the vanadate and PhAH complexes compared to any of the other enzyme species and are shifted to lower field relative to the native enzyme. There are also abundant and well-resolved hyperfine lines observed in the region from 0.3 to 3.0 kG. These hyperfine lines can be attributed to the dinuclear $(Mn^{2+})_2$ species as they exhibit ca. 40 G spacing. In the vanadate complex, superhyperfine interactions between the spin of the unpaired electron and the nuclear spin of ^{51}V ($I = 7/2$) are also possible. For $J \gg A$, the number of hyperfine lines expected for a Mn^{2+} dimer is $2nI + 1 = 11$, whereas 15 hyperfine lines are possible for the interaction with ^{51}V, giving a total of 165 possible hyperfine lines. In the region from 0.5 to 3.0 kG, >50 hyperfine lines can easily be resolved, although whether they result from hyperfine coupling to the spin-coupled $(Mn^{2+})_2$ dimer as well as a superhyperfine interaction with an outer-sphere ^{51}V nucleus cannot be determined at this stage.

DISCUSSION

In recent years, it has been determined that the PPP family of metallophosphatases utilizes a dinuclear metal center for catalysis (*1*−*4*, *19*, *44*) and transfers the phosphoryl group from substrate phosphomonoesters directly to water without the formation of a phosphoenzyme intermediate (*27*, *45*). Kinetic isotope effect studies of calcineurin (*46*, *47*) and λPP (*48*) indicated a dissociative mechanism in which significant P−O bond cleavage occurs in the transition state with significant buildup of negative charge on the leaving group. These studies also determined that the dianion was the substrate of the reaction. A number of other studies have implicated a metal-coordinated solvent as the nucleophile (*44*, *49*−*51*), consistent with the elegant work of Chin and colleagues on a dinuclear Co^{3+} model complex (*52*). Yet other studies have raised the intriguing possibility of an outer-sphere mechanism for the nucleophilic solvent molecule (*53*). Based on the X-ray structure of the phosphate-inhibited form of PP2C, which shows phosphate bound but not directly coordinated to either metal ion, an outer-sphere mechanism may also be considered for that enzyme, a member of the PPM metallophosphatase family (*54*).

Mechanistic details that are not well understood include the means by which the dinuclear metal ion cofactor interacts with substrate, transition state, and product(s) throughout the catalytic cycle. Several roles have been postulated for the metal ions during catalysis including activation of the solvent

nucleophile to lower its pK_a; neutralization of the negative charge on the phosphoryl group oxygens by complexation, making the phosphorus atom more electrophilic and prone to nucleophilic attack; and charge neutralization of the leaving group. In addition, the metal ions may position substrate and solvent for optimal nucleophilic attack or may interact with the transition state to lower its energy. A variety of spectroscopic studies have demonstrated that oxoanions (phosphate and phosphate analogues) interact with the dinuclear metal center by direct complexation to the metal ions (*28*−*30*, *55*−*60*). Although the most common coordination mode has the tetrahedral oxoanion binding in a symmetrically bridged fashion to both metal ions (*4*, *19*, *32*−*34*), two novel geometries (terminal/monodentate and bridged/tridentate) were recently revealed in the sulfate complex of λPP. In addition, an unsymmetrical binding mode was observed for the molybdate and tungstate complexes of FeZn uteroferrin (*57*). A study into how Mn^{2+}-activated λPP is inhibited by organic and orthophosphate analogue inhibitors is presented in order to gain further insight into the catalytic mechanism.

The small organic anion PhAH was found to be a potent inhibitor ($K_i = 5.1 \pm 1.6$ μM) and a useful probe in further characterizing the symmetry and electron environment of the spin-coupled dinuclear [$(Mn^{2+})_2$] cluster of λPP. PhAH was synthesized by Anderson and Cleland to be a reaction intermediate analogue for enolase, the enzyme that catalyzes the reversible dehydration of 2-phospho-D-glyerate to give phosphoenolpyruvate (*61*). Enolase utilizes a dinuclear $(Mg^{2+})_2$ active site cofactor, but Mn^{2+} can also substitute and has proven to be a useful paramagnetic probe (*62*, *63*). In the presence of saturating Mg^{2+}, PhAH is a slow, tight binding inhibitor of enolase, with a $K_i = 15$ pM (*37*). EPR measurements of Mn^{2+}−enolase in the presence of various ^{17}O-labeled forms of PhAH revealed a bichelate structure of the inhibitor, in which the carbonyl oxygen of the hydroxamate is a μ-bridging ligand (*62*), a result that was confirmed by determining the X-ray structure of the PhAH−enolase complex (*61*, *63*). We propose that PhAH binds to the active site of λPP in a similar fashion. Thus, an oxygen atom from the phosphonate group may be terminally coordinated to one Mn^{2+} ion, the carbonyl oxygen atom of the hydroxamate group replaces the μ-aquo/hydroxo ligand, and a terminally coordinated solvent molecule on the other Mn^{2+} ion may be substituted with the hydroxamate oxygen atom (Scheme 1). Besides the known propensity for phosphonate and hydroxamate groups for metal complexation, the formation of thermodynamically favorable 5- and 6-membered rings involving PhAH and both M1 and M2 metal ions makes the structure in Scheme 1 seem quite reasonable. In Scheme 1, we have placed the phosphonate group to coordinate to the high-affinity M2 metal ion (*22*) to be analogous to the terminal sulfate anion in the unit cell A and B molecules in the recent X-ray structure of λPP (*1*). Since there is no crystal structure of PhAH complexed to λPP, the proposed binding mode shown in Scheme 1 is tentative, especially considering the differences in affinity and kinetics regarding the way PhAH interacts with λPP versus enolase. The EPR spectra of the enolase−Mn^{2+}−PhAH complex were time-dependent, and it has been speculated that this may be related to the slow binding inhibition behavior (*62*). Nevertheless, structural elements

Scheme 1: Model of PhAH Bound to the Active Site of λ Protein Phosphatase

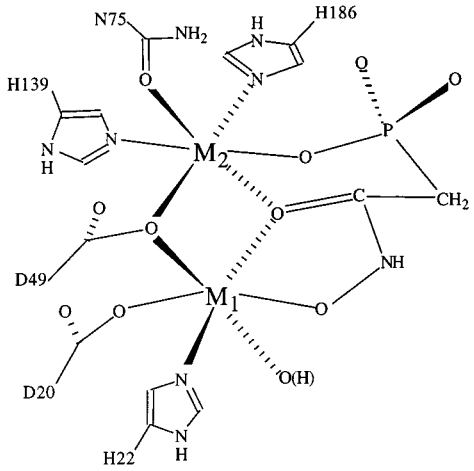

responsible for the slow binding behavior of PhAH to enolase were not apparent in three-dimensional structures of enolase (*63*, *64*). In light of this comparison, placement of the carbonyl oxygen atom as a μ-bridging ligand is consistent with our EPR studies which indicate a decrease in the exchange coupling constant. Ongoing spectroscopic analyses will hopefully resolve more details regarding the structure of the λPP−PhAH inhibitor complex.

Phosphatase inhibition kinetics of λPP with Mn^{2+} reveal that the product of the dephosphorylation reaction, phosphate, and other oxoanion inhibitors including orthovanadate, molybdate, tungstate, arsenate, and sulfate, all exhibit competitive inhibition. Furthermore, EPR spectra indicate that all oxoanion inhibitors directly interact and perturb the ligand field environment of the dinuclear $(Mn^{2+})_2$ cluster of λPP. These oxoanion inhibitors also decrease the exchange coupling between the two paramagnetic Mn^{2+} ions, indicating a perturbation to the bridging ligand. Nevertheless, the K_i values for these molecules differ by over 5 orders of magnitude. Although one reason for the low affinity of sulfate dianion for Mn^{2+}-reconstituted λPP could be attributed to its short sulfur−oxygen bond lengths, there is no apparent trend in the K_i value when compared to the X−O bond lengths of the various oxoanions noted in Table 1. Similarly, although the pK_a values for these oxoanions differ considerably, all oxoanions exist primarily as a dianion at the pH studied (pH 7.8).

The geometry of phosphate, sulfate, and arsenate is usually considered to be tetrahedral, and each has only a limited capability to undergo a change in coordination geometry. This is certainly the case when examining a number of X-ray structures, e.g., the phosphate, tungstate, and sulfate complexes of calcineurin, purple acid phosphatase, PP1, and λPP (*1*, *2*, *4*). Nevertheless, in some structures of low resolution, it may not be possible to determine the exact geometry about the oxoanion central atom. More recently, high-resolution X-ray structures have indicated that some oxoanions are capable of expanding their coordination number. For example, the 1.9 Å structure of alkaline phosphatase complexed with vanadate indicates that the vanadium atom adopts a trigonal bipyramidal geometry by forming a covalent bond with the active site serine nucleophile (*31*). A similar covalent trigonal bipyramidal geometry for vanadium was observed

in the vanadate-inhibited form of the low molecular weight tyrosine phosphatase from bovine heart. In that structure, vanadate formed a covalent linkage to an active site cysteine residue (*65*). Interestingly, a crystal structure in the presence of molybdate was also formed in this study. The molybdate complex was found to exhibit simple tetrahedral geometry, and a reported K_i value of 1.4 ± 0.4 mM was observed. Similar to the trend reported in this study, the K_i value for molybdate was 10^3 times greater than the K_i for vanadate ($K_i = 1.0 \pm 0.6$ μM). In both studies, it was hypothesized that the trigonal bipyramidal structure represented a transition state along the reaction pathway. Additional evidence for vanadate expanding its coordination sphere to five is also observed in a 1.9 Å resolution crystal structure of a vanadate-trapped ADP complex of *Dictyostelium* myosin(II) (*66*). Here, vanadate is modeled as trigonal bipyramidal within the γ- phosphate binding pocket of ATP, with three short, equatorial V−O bond lengths of 1.6−1.7 Å and two longer ones at 2.1−2.3 Å. Although this is a hydrolysis reaction involving a phosphoanhydride, i.e., ATP, the mechanism of phosphoryl transfer is reminiscent of that expected for the PPPs. Although fewer structures are known with tungstate coordinated at the active site, it has been shown that this oxoanion can also increase its coordination number to 5. A pentacoordinated tungstate ion with trigonal bipyramidal geometry is observed in the adenosine−tungstate complex of the fragile histidine triad (FHIT) protein (*67*).

Keeping these results in mind, we hypothesize that the large range of inhibition constants for the various oxoanions can be explained by the differences in oxoanion geometry when complexed to the active site dinuclear metal center of λPP and the ability of these ions to rapidly and reversibly form chelates at the active site dinuclear metal center of λPP. The higher affinity of vanadate and tungstate may very well be due to the abilities of these oxoanions to expand their coordination number, forming trigonal bipyramidal geometries with a metal-coordinated solvent molecule. Alternatively, the oxoanions may remain tetrahedral but coordinate differently to the dinuclear metal center. It is worth noting the similarities between the EPR spectra of PhAH-, tungstate-, and vanadate-inhibited λPP (Figure 2, D, E, and F). If PhAH interacts with the dinuclear $(Mn^{2+})_2$ center of λPP via a bridging carbonyl oxygen atom as proposed in Scheme 1, it could also indicate that vanadate and tungstate bind by providing a μ-oxygen bridge as well. Without a doubt, a high-resolution structure of λPP complexed with PhAH, vanadate, or tungstate could provide a wealth of mechanistic information.

ACKNOWLEDGMENT

We gratefully acknowledge Debbie C. Crans for insightful discussions and helpful experimental suggestions and George H. Reed and Russel R. Poyner for thoughtful comments regarding the interaction of PhAH with enolase. We thank John Enemark for providing reference material on the chemical properties of oxometalates.

SUPPORTING INFORMATION AVAILABLE

Supporting Information is available for plots of velocity versus substrate concentration in the presence and absence of inhibitor for λPP and of the time dependence inhibition of λPP by PhAH. This information is available free of charge via the Internet at http://pubs.acs.org.

REFERENCES

1. Voegtli, W. C., White, D. J., Reiter, N. J., Rusnak, F., and Rosenzweig, A. C. (2000) *Biochemistry 39*, 15365−15374.
2. Kissinger, C. R., Parge, H. E., Knighton, D. R., Lewis, C. T., Pelletier, L. A., Tempczyk, A., Kalish, V. J., Tucker, K. D., Showalter, R. E., Moomaw, E. W., Gastinel, L. N., Habuka, N., Chen, X., Maldonado, F., Barker, J. E., Bacquet, R., and Villafranca, J. E. (1995) *Nature 378*, 641−644.
3. Goldberg, J., Huang, H., Kwon, Y., Greengrad, P., Nairn, A. C., and Kuriyan, J. (1995) *Nature 376*, 745−753.
4. Egloff, M.-P., Cohen, P. T. W., Reinemer, P., and Barford, D. (1995) *J. Mol. Biol. 254*, 942−959.
5. Lohse, D. L., Denu, J. M., and Dixon, J. E. (1995) *Structure 3*, 987−990.
6. Leng, J., Cameron, A. J., Buckel, S., and Kennelly, P. J. (1995) *J. Bacteriol. 177*, 6510−6517.
7. Potts, M., Sun, H., Mockaitis, K., Kennelly, P. J., Reed, D., and Tonks, N. K. (1993) *J. Biol. Chem. 268*, 7632−7635.
8. DePaoli-Roach, A. A., Park, I.-K., Cerovsky, V., Csortos, C., Durbin, S. D., Kuntz, M. J., Sitikov, A., Tang, P. M., Verin, A., and Zolmierowicz, S. (1994) *Adv. Enzyme Regul. 34*, 199−224.
9. Shenolikar, S., and Nairn, A. C. (1991) *Adv. Second Messenger Phosphoprotein Res. 23*, 3−121.
10. Rusnak, F., and Mertz, P. (2000) *Physiol. Rev. 80*, 1483−1521.
11. Aramburu, J., Rao, A., and Klee, C. B. (2000) *Curr. Top. Cell. Regul. 36*, 237−295.
12. Cohen, P. T. W. (1994) *Adv. Protein Phosphatases 8*, 371−376.
13. Ingebritsen, T. S., and Cohen, P. (1983) *Science 221*, 331−338.
14. Cohen, P., and Cohen, P. T. W. (1989) *J. Biol. Chem. 264*, 21435−21438.
15. Cohen, P. (1989) *Annu. Rev. Biochem. 58*, 453−508.
16. Rusnak, F., Yu, L., and Mertz, P. (1996) *JBIC 1*, 388−396.
17. Barton, G. J., Cohen, P. T. W., and Barford, D. (1994) *Eur. J. Biochem. 220*, 225−237.
18. Koonin, E. V. (1994) *Protein Sci. 3*, 356−358.
19. Griffith, J. P., Kim, J. L., Kim, E. E., Sintchak, M. D., Thomson, J. A., Fitzgibbon, M. J., Fleming, M. A., Caron, P. R., Hsiao, K., and Navia, M. A. (1995) *Cell 82*, 507−522.
20. Zhuo, S., Clemens, J. C., Hakes, D. J., Barford, D., and Dixon, J. E. (1993) *J. Biol. Chem. 268*, 17754−17761.
21. Rusnak, F., Yu, L., Todorovic, S., and Mertz, P. (1999) *Biochemistry 38*, 6943−6952.
22. White, D. J., Reiter, N. J., Sikkink, B. S., Yu, L., and Rusnak, F. (2001) *Biochemistry 40*, 8918−8929.
23. Zhuo, S., Clemens, J. C., Stone, R. L., and Dixon, J. E. (1994) *J. Biol. Chem. 269*, 26234−26238.
24. Vincent, J. B., Crowder, M. W., and Averill, B. A. (1991) *Biochemistry 30*, 3025−3034.
25. Doi, K., Gupta, R., and Aisen, P. (1987) *J. Biol. Chem. 262*, 6982−6985.
26. Chasteen, N. D. (1983) *Struct. Bonding 53*, 105−138.
27. Martin, B. L., and Graves, D. J. (1986) *J. Biol. Chem. 261*, 14545−14550.
28. David, S. S., and Que, L., Jr. (1990) *J. Am. Chem. Soc. 112*, 6455−6464.
29. Vincent, J. B., Crowder, M. W., and Averill, B. A. (1992) *Biochemistry 31*, 3033−3037.
30. Crans, D. C., Simone, C. M., Holz, R. C., and Que, L., Jr. (1992) *Biochemistry 31*, 11731−11739.
31. Holtz, K. M., Stec, B., and Kantrowitz, E. R. (1999) *J. Biol. Chem. 274*, 8351−8354.
32. Klabunde, T., Strater, N., Frohlich, R., Witzel, H., and Krebs, B. (1996) *J. Mol. Biol. 259*, 737−748.
33. Uppenberg, J., Lindqvist, F., Svensson, C., Ek-Pylander, B., and Andersson, G. (1999) *J. Mol. Biol. 290*, 201−211.

34. Guddat, L. W., McApline, A. S., Hume, D., Hamilton, S., de Jersey, J., and Martin, J. L. (1999) *Structure 7*, 757−767.
35. Lindqvist, Y., Johansson, E., Kaija, H., Vihko, P., and Schneider, G. (1999) *J. Mol. Biol. 2*, 135−147.
36. Tabor, S., and Richardson, C. C. (1985) *Proc. Natl. Acad. Sci. U.S.A. 82*, 1074−1078.
37. Anderson, V. E., Weiss, P. M., and Cleland W. W. (1984) *Biochemistry 23*, 2779−2786.
38. Pope, M. T., and Müller, A. (1991) *Angew. Chem., Int. Ed. Engl. 30*, 334−348.
39. Crans, D. C., Willging, E. M., and Butler S. R. (1990) *J. Am. Chem. Soc. 112*, 427−432.
40. Pope, M. T. (1983) *Heteropoly and Isopoly Oxometalates*, Vol. 8, Springer-Verlag, New York.
41. Kuzmic, P. (1996) *Anal. Biochem. 237*, 260−273.
42. Reed, G. H., and Markham, G. D. (1984) *Biol. Magn. Reson. 6*, 73−142.
43. Howard, T., Telser, J., and DeRose V. J. (2000) *Inorg. Chem. 39*, 3379−3385.
44. Yu, L., Haddy, A., and Rusnak, F. (1995) *J. Am. Chem. Soc. 117*, 10147−10148.
45. Mueller, E. G., Crowder, M. W., Averill, B. A., and Knowles, J. R. (1993) *J. Am. Chem. Soc. 115*, 2974−2975.
46. Hengge, A. C., and Martin, B. L. (1997) *Biochemistry 36*, 10185−10191.
47. Martin, B. L., Jurado, L. A., and Hengge, A. C. (1999) *Biochemistry 38*, 3386−3392.
48. Hoff, R. H., Mertz, P., Rusnak, F., and Hengge, A. C. (1999) *J. Am. Chem. Soc. 121*, 6382−6390.
49. Aquino, M. A. S., Lim, J.-S., and Sykes, G. A. (1994) *J. Chem. Soc., Dalton Trans.*, 429−436.
50. Yu, L., Golbeck, J., Yao, J., and Rusnak, F. (1997) *Biochemistry 36*, 10727−10734.
51. Wang, X., Ho, R. Y. N., Whiting, A. K., and Que, L., Jr. (1999) *J. Am. Chem. Soc. 121*, 9235−9236.
52. Wahnon, D., LeBuis, A.-M., and Chin, J. (1995) *Angew. Chem., Int. Ed. Engl. 34*, 2412−2414.
53. Merkx, M., and Averill, B. A. (1999) *J. Am. Chem. Soc. 121*, 6683−6689.
54. Das, A. K., Helps, N. R., Cohen, P. T. W., and Barford, D. (1996) *EMBO J. 15*, 6798−6809.
55. True, A. E., Scarrow, R. C., Randall, C. R., Holz, R. C., and Que, L., Jr. (1993) *J. Am. Chem. Soc. 115*, 4246−4255.
56. Pinkse, M. W. H., Merkx, M., and Averill, B. A. (1999) *Biochemistry 38*, 9926−9936.
57. Wang, W., and Que, L., Jr. (1998) *Biochemistry 37*, 7813−7821.
58. Priggemeyer, S., Eggers-Borkenstein, P., Ahlers, F., Henkel, G., Korner, M., Witzel, H., Nolting, H.-F., Hermes, C., and Krebs, B. (1995) *Inorg. Chem. 34*, 1445−1454.
59. Dietrich, M., Munstermann, D., Suerbaum, H., and Witzel, H. (1991) *Eur. J. Biochem. 199*, 105−113.
60. Wang, D. L., Holz, R. C., David, S. S., Que, L., Jr., and Stankovich, M. T. (1991) *Biochemistry 30*, 8187−8194.
61. Reed, G. H., Poyner, R. R., Larsen, T. M., Wedekind, J. E., and Rayment, I. (1996) *Curr. Opin. Struct. Biol. 6*, 736−743.
62. Poyner, R. R., and Reed, G. H. (1992) *Biochemistry 31*, 7166−7173.
63. Wedekind, J. E., Poyner, R. R., Reed, G. H., and Rayment, I. (1994) *Biochemistry 33*, 9333−9342.
64. Larsen, T. M., Wedekind, J. E., Rayment, I., and Reed, G. H. (1996) *Biochemistry 35*, 4349−4358.
65. Zhang, M., Zhou, M., Van Etten, R. L., and Stauffacher, C. V. (1997) *Biochemistry 36*, 15−23.
66. Smith, C. A., and Rayment, I. (1996) *Biochemistry 35*, 5404−5417.
67. Lima, C. D., Klein, M. G., and Hendrickson, W. A. (1997) *Science 278*, 286−289.
68. Tsai, Y.-M., Wang, S.-L., Huang, C.-H., and Lii, K.-H. (1999) *Inorg. Chem. 38*, 4183−4187.
69. Ekambaram, S., and Sevov, S. C. (2000) *Inorg. Chem. 39*, 2405−2410.
70. Bazan, B., Mesa, J. L., Pizarro, J. L., Lezama, L., Arriortua, M. I., and Rojo, T. (2000) *Inorg. Chem. 39*, 6056−6060.
71. Hsu, K.-F., and Wang, S.-L. (1998) *Inorg. Chem. 37*, 3230−3235.
72. Smith, R. M., and Martel, A. E. (1989) in *Critical Stability Constants*, Plenum Press, New York.

BI011577B